

Spitzer Mid-infrared Study of Compact H II Regions in the Magellanic Clouds

V. Charmandaris^{1,2,3}, M. Heydari-Malayeri³, and E. Chatzopoulos¹

¹ University of Crete, Department of Physics, Heraklion, GR-71003, Greece
e-mail: vassilis@physics.uoc.gr

² IESL/Foundation for Research and Technology - Hellas, GR-71110, Heraklion, Greece

³ Observatoire de Paris, LERMA, 61 Avenue de l'Observatoire, F-75014, Paris, France

Received February 27, 2008; accepted May 16, 2008

ABSTRACT

Aims. We present a study of the mid-infrared properties and dust content of a sample of 27 H II “blobs”, a rare class of compact H II regions in the Magellanic Clouds. A unique feature of this sample is that even though these H II regions are of high and low excitation they have nearly the same physical sizes $\sim 1.5\text{--}3$ pc.

Methods. We base our analysis on archival $3\text{--}8\ \mu\text{m}$ infrared imagery obtained with the Infrared Array Camera (IRAC) on board the Spitzer Space Telescope.

Results. We find that despite their youth, sub-solar metallicity and varied degrees of excitation, the mid-infrared colors of these regions are similar to those of typical H II regions. Higher excitation “blobs” (HEBs) display stronger $8\ \mu\text{m}$ emission and redder colors than their low-excitation counterparts (LEBs).

Key words. (ISM:) H II regions – (ISM:) dust, extinction – Infrared: ISM – Infrared: star – (Galaxies:) Magellanic Clouds

1. Introduction

The detailed study of massive star formation in galaxies has been a challenging research area over the years. Two of the main reasons are that massive stars are intrinsically rare and their lifetime is short (see Zinnecker & Yorke, 2007, for a review). In addition they are predominantly formed not in isolation but in tight groups in dense molecular clouds, where they are enshrouded by large quantities of dust. As a result, probing massive stars at their early stages of evolution is particularly difficult, since they are not readily observed in the ultraviolet and optical wavelengths which give direct access to their physical parameters. At this stage they can only be detected indirectly by their infrared and radio emission, which is due to emission from the surrounding dust and the associated ionized H II region respectively. As massive stars evolve though, their far-UV photons and strong winds dissociate the molecules in the surrounding clouds and ionize the atoms creating ultra-compact H II regions. Eventually, the natal molecular cloud is fully ionized to become a compact H II region. As the front expands and the volume of the ionized gas increases, the advancing ionization front of the H II region reaches the outer surface of the molecular cloud. Then the ionized gas flows away into the interstellar medium according to the so-called champagne effect (Tenorio-Tagle, 1979; Bodenheimer et al., 1979) and consequently the newborn stars become accessible to observation in the ultraviolet and visible.

A number of very young, emerging H II regions were identified in the Magellanic Clouds on the basis of ground-based observations at the European Southern Observatory, nearly 20 years ago (Heydari-Malayeri & Testor, 1982, 1983, 1985, 1986; Heydari-Malayeri et al., 1990; Testor & Pakull, 1985; Heydari-Malayeri et al., 1988a). Searching for this type of regions in the Magellanic Clouds was motivated by the fact

that the interstellar extinction along this line of sight is lower than towards the disk of our Galaxy and that the lower metallicity of the Small and Large Magellanic Clouds (SMC and LMC respectively) favors the formation of massive stars (Wolfire & Cassinelli, 1987; Melena et al., 2008).

This distinct and very rare class of H II regions in the Magellanic Clouds was called H II “blobs” since no features could be distinguished with the available telescopes at the time. They were classified as high-excitation and low-excitation compact H II “blobs” (HEBs and LEBs respectively), principally based on the temperature and mass of their exciting stars, as well as their nebular H β luminosity (for details see Meynadier & Heydari-Malayeri, 2007). Contrary to the typical H II regions of the Magellanic Clouds, which are extended structures with sizes of several arc minutes corresponding to physical scales of more than 50 pc and powered by a large number of exciting stars, HEBs and LEBs are dense and small regions of $\sim 5''$ to $10''$ in diameter in the optical, corresponding to $\sim 1.5\text{--}3.0$ pc. Studies in the optical reveal that they are heavily affected by local dust (Heydari-Malayeri et al., 1988a; Israel & Koornneef, 1991). A noteworthy characteristic of the HEBs is that they harbor the youngest massive stars accessible to infrared and optical observations. Since for massive stars the accretion time-scale is larger than the Kelvin-Helmholtz time-scale, they reach the main sequence while accretion is still taking place. Moreover, as pointed out before, massive stars evolve very fast and as a result obtaining their physical parameters “at birth” is a fairly challenging task! It is now believed that the “blobs” correspond to the final stages in the evolution of the ultra-compact H II regions, whose Galactic counterparts are detected only at infrared and radio frequencies (Churchwell, 1990). The study of HEBs thus bridges a gap between understanding the properties of completely dust enshrouded stars inside ultra-

compact H II regions and those of the exciting stars in evolved H II regions (Heydari-Malayeri et al., 2007). It should be noted that an important characteristic of our compact H II region sample is their uniform physical size which varies by less than a factor of two among all “blobs”. This additional constraint makes them an ideal laboratory to study problems related to the formation of massive stars and their environment within a well defined region. Because of the contamination by strong nebular background no direct information about the number of the exciting stars of the blobs was possible with ground-based telescopes. A detailed high spatial resolution imaging and spectroscopy campaign of a number of those regions was performed with the Hubble Space Telescope and several of those issues were addressed (see Heydari-Malayeri et al., 1999, 2003, 2007, and references therein).

The complex interaction between the ionizing radiation of the young stars, their dusty cocoons and adjacent molecular clouds can be best studied in mid-infrared (mid-IR) wavelengths. At this wavelength range, not only we are less affected by extinction, but also a number of ionization lines (such as [S IV] $10.51 \mu\text{m}$, [Ne II] $12.81 \mu\text{m}$, [Ne III] $15.55 \mu\text{m}$.) which probe the chemistry the interstellar gas and radiation field are available. Furthermore, the strength of broad spectral features, such as those emitted by Polycyclic Aromatic Hydrocarbons (PAHs) are readily accessible and these can be used to trace the properties of the surrounding dust and molecules as well as estimate the star formation rate (see Peeters et al., 2002; Förster Schreiber et al., 2004; van Dishoeck, 2004; Calzetti et al., 2007, and references therein).

A number of authors have already explored the mid-IR properties of H II regions in the Magellanic Clouds with the Infrared Space Observatory (ISO) and with the Spitzer Space Telescope (i.e. Vermeij et al., 2002; Jones et al., 2005; Gouliermis et al., 2007; Lebouteiller et al., 2007). None of those studies though examined the compact H II region sample as a whole with sufficient spatial resolution. The more detailed spectroscopic study of Vermeij et al. (2002) used ISO/PHOT-S to explore the variation of the PAH features in the 5.8 to $11.6 \mu\text{m}$ range. This work did reveal some interesting correlations between the strength of the PAH features, as well as a difference in the total PAH emission normalized by the strength of the radiation field between H II regions in the Magellanic Clouds and those in our Galaxy. However, the ISO aperture used was rather large ($24'' \times 24''$) and the spectra clearly included not only the emission from the “blobs” but also from adjacent star forming and photo-dissociation regions.

Here we present for the first time a mid-IR high resolution study of the HEBs and LEBs in the 3.6 to $8.0 \mu\text{m}$ range based on archival Spitzer Space Telescope imagery. This is a natural extension of the optical and near-IR studies of the sample already performed by our group (see Heydari-Malayeri et al., 2007; Meynadier & Heydari-Malayeri, 2007, and references therein) which were concentrated on the stellar content and excitation mechanisms of the ionized gas. The present work is focused on the so far unexplored mid-IR colors and morphology of these objects. This complete multi-wavelength coverage should facilitate the comparison of the object properties in various wavelengths, and enable a more realistic modeling of these objects in the future. Given the direct coupling between gas, dust, and star formation, the Spitzer data present new possibilities in understanding the physics of obscured dust enshrouded regions. It is thus instructive to contrast the compact and normal H II region samples in mid-IR.

We perform photometry using a circular aperture of $\sim 7''$ in diameter, which corresponds to a size of ~ 2 pc at the distance of the LMC and SMC. The aperture size is based on the fact that comparison between the mid-IR and optical images showed that the sample objects are always less extended in the mid-IR band. A total of 27 blobs from the sample analyzed in Meynadier & Heydari-Malayeri (2007) were in areas of the Magellanic clouds where high quality Spitzer imaging data were publicly available. A particularity of this study is that it deals with a sample of compact H II region which have comparable physical sizes. In Section 2 we present the sample and the Spitzer observations, and in Section 3 we discuss our main results. We discuss our findings in the context of similar studies of giant H II regions and young dust enshrouded protostars in Section 4, and close with our conclusion in Section 5.

2. Observations and Data Reduction

The data used for this study were obtained with the Infrared Array Camera (IRAC) (Fazio et al., 2004) instrument on board the Spitzer Space Telescope (Werner et al., 2004) and were recovered from Spitzer Archive. The observations of the Large Magellanic Cloud (LMC) were part of the Spitzer Legacy project “Surveying the Agents of a Galaxy’s Evolution” (SAGE, PI M. Meixner, PID = 20203, see Meixner et al. 2006), while the Small Magellanic Cloud data were observed by the GO program of A. Bolatto (PID = 3316, see Bolatto et al. 2007). A total of 24 sec of on-source observing time per filter was devoted for each sky position at the LMC using 12 sec frames and a raster which resulted in two frames per position. The SMC data were obtained using 12sec frames and a 3 position dither producing an on source exposure of a total of 36 sec. The data were processed with the Spitzer Science Center (SSC) pipeline (version 14.0.0) which created the final mosaics used for our analysis.

All 27 sources were identified visually based on accurate coordinates and after cross-checking their position with existing optical observations. As an example of the quality of the data we present in Fig. 1 an image of the general area in the LMC which contains the HEB N11A. Photometry was performed using the “aper” IDL routine with circular apertures of 3 pixels ($3.6''$) in radius and the corresponding flux correction factors for the extended size of the PSF described in the IRAC data handbook were applied. Special care was devoted to proper background subtraction as some of the sources were in crowded fields. The absolute errors in photometry are at the 5% level. Our photometric results are presented in Table 1, which gives the target ID used in Figs. 3 and 4, the RA and Dec of the target identified in the IRAC images, and the Spitzer observation AORKEY. A few sources of the original sample, presented in Meynadier & Heydari-Malayeri (2007), which were saturated or unresolved in the Spitzer images were not included in this study. In Table 1 we also provide the 1σ of the variation of the sky (in MJy sr^{-1}) next to each target.

3. Results

The analysis of the IRAC images of the regions resulted in identification of point sources in the expected locations of the HEBs and LEBs. Despite the improved Spitzer resolution, the size of the IRAC point spread function (FWHM $\sim 2.5''$ at $8 \mu\text{m}$) does not permit a direct comparison with the sub-arc-second resolution of the *HST* optical images or the deconvolved VLT near-IR imagery available (i.e. Heydari-Malayeri et al., 1999, 2003). For

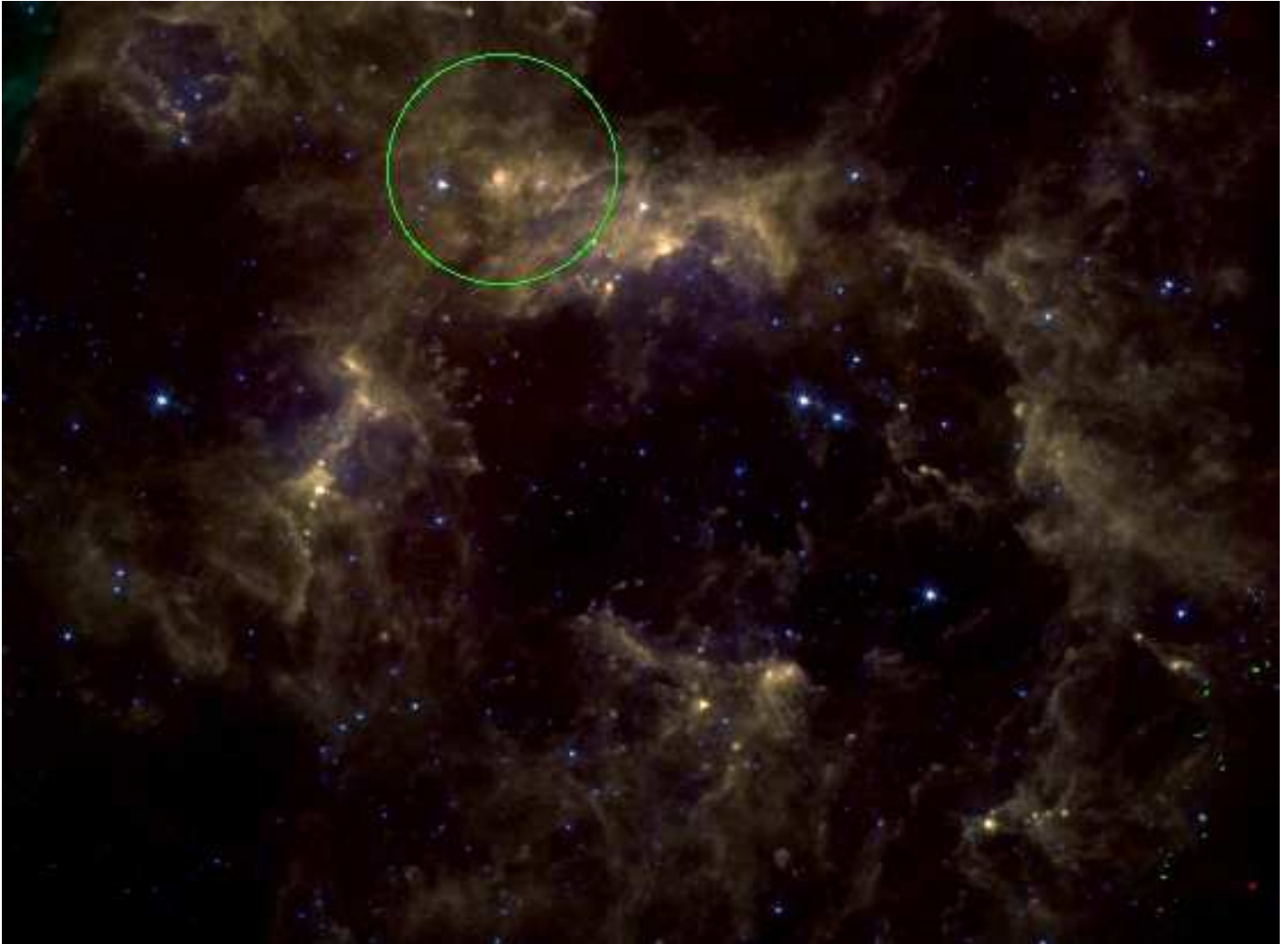


Fig. 1. A “true color” image of the Large Magellanic Cloud giant H II region N11. A circle of 2 arcmin in radius is centered on the compact H II region N11A, which lies on the northern ridge of a giant shell surrounding a cavity created by massive stars in its central regions. The composite image was created by combining the three 3.6, 5.8, and 8.0 μm bands into a blue-green-red frame. The image size is $\sim 22.8 \times 9.0$ arcmin, corresponding to $\sim 410 \times 162$ pc at the distance of the LMC. North is up and East is to the left.

example, Fig. 1 presents the LMC high-excitation blob N11A, which can be compared with the *HST* image of this object (see Heydari-Malayeri et al., 2001, for a detailed analysis). A series of close-up images of LMC-N11A is also presented in Fig. 2. One can identify some of the exciting stars visible in the *HST* B-band Fig. 2a image, as well as the turbulent environment surrounding them, shaped by their strong stellar winds, visible by the $\text{H}\alpha$ emission displayed in Fig. 2b. In addition, we include in Fig. 2c and Fig. 2d the Spitzer 3.6 and 8 μm images of the N11A. Even though we do detect some diffuse emission around the region, more than 90% of the flux originates from the central “blob”, and it well sampled by our photometry aperture. Thus, for the purpose of this study, we shall consider all compact H II regions as unresolved to this scale.

To explore the mid-IR properties of our sample we constructed the typical IRAC magnitude and color-color diagrams presented in Fig. 3 and 4 and discussed in detail in the following section. In Fig. 3 we display the 8 μm flux of the regions as a function of their [3.6]-[8.0] color, with their ID, as indicated in Table 1. A box marked with dashed lines indicates the expected locus of normal giant H II regions at the mean distance

of the Magellanic Clouds (Whitney et al., 2004; Meixner et al., 2006; Gouliermis et al., 2007). In addition, the general location where low-mass young stellar objects (YSOs), Class I and Class II, have been found (based on observations presented by Cohen, 1993, 2007; Gouliermis et al., 2007) are also marked with the hatched rectangular areas. We observe that overall both HEBs and LEBs are found in the areas of the diagram where normal extended H II regions and Class II protostars are located. This aspect will be discussed in the following Section. Furthermore, the HEBs are in general more luminous than the LEBs and that the most luminous ones are also the reddest. This is in line with previous results from optical spectroscopy implying that HEBs are younger than LEBs (Meynadier & Heydari-Malayeri, 2007). We note also that the variation of the mid-IR luminosity at 8 μm versus the [3.6] - [8.0] color can be roughly approximated with a linear fit.

4. Discussion

Generally speaking, the mid-IR fluxes do not directly originate from the exciting stars of the corresponding H II region, as photospheric emission from individual OB stars at the distance of the

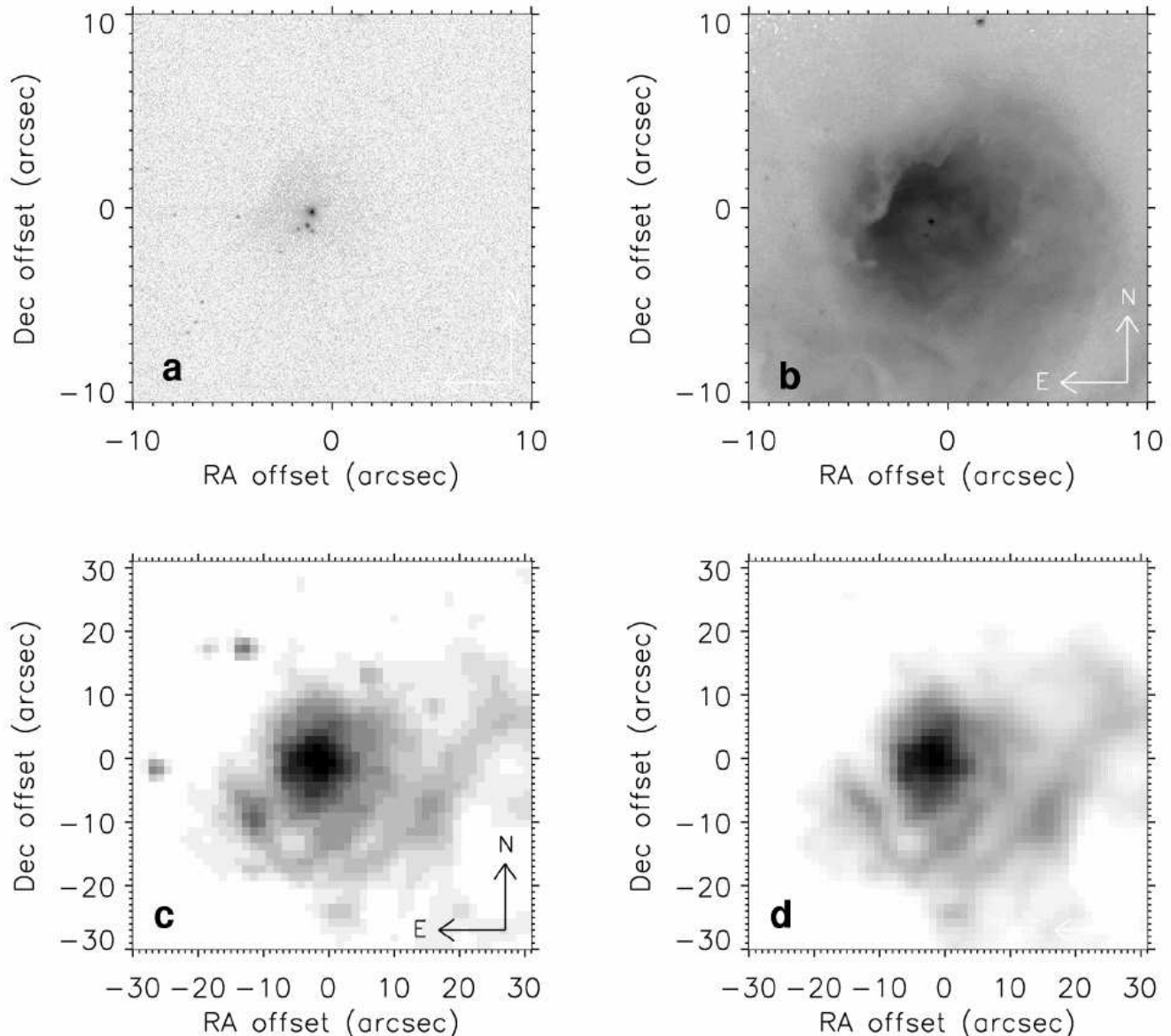


Fig. 2. A mosaic of four close-up images of the LMC high-excitation region N11A presented in Fig. 1. North is up, East is to the left, and the center of the field is at RA=4:57:16.2, Dec=-66:23:20.8 (J2000). The upper-row images were obtained with *HST* (see Heydari-Malayeri et al., 2001) and the lower-row ones with *Spitzer*. *a*) B-band image obtained with the F410M filter of WFPC2. A few of the central exciting stars are visible. *b*) H α image of N11A. Notice the turbulent environment surrounding the central source, the filamentary structure due to dust extinction and the ionization front from the north west. *c*) A *Spitzer*/IRAC 3.6 μ m image of N11A. Even though extended emission is detected, the bulk of the light is well encompassed within our aperture. *d*) Same as in *c*) but for the *Spitzer*/IRAC 8 μ m image.

Magellanic Clouds is too faint in the [8.0] μ m band to be measured (Jones et al., 2005). The 8 μ m IRAC filter probes mostly reprocessed emission from the 7.7 μ m PAH feature which is produced in the photo-dissociation regions (PDRs) surrounding star forming regions (ie Peeters et al., 2002). The HEBs have higher 8 μ m fluxes than the LEBs because the former harbor hotter, more massive stars whose ionizing radiation can penetrate deeper into the PDRs producing more PAH feature emission.

Moreover, as pointed out previously, the HEBs are younger and therefore are found in areas with larger quantities of gas and dust. These two factors contribute to the observed linear relationship between the 8 μ m flux and the [3.6] – [8.0] color. In addition

to the elevated PAH emission from the PDRs falling within our apertures, the 8 μ m flux, along with the 4–12 μ m slope can also increase substantially due to emission from very small grains. These grains have a radius less than 10 nm and are prominent in Galactic H II regions (Verstraete et al., 1996; Cesarsky et al., 1996) as well as in deeply embedded extragalactic giant H II regions (i.e. Mirabel et al., 1998).

Overall the LMC HEBs are more luminous and more dusty than their SMC counterparts. Previous observations, using both ground-based telescopes and *HST*, have shown N88A (object #14) to be an outstanding compact H II region in the SMC as far as its luminosity and dust content are concerned. Fig. 3 confirms

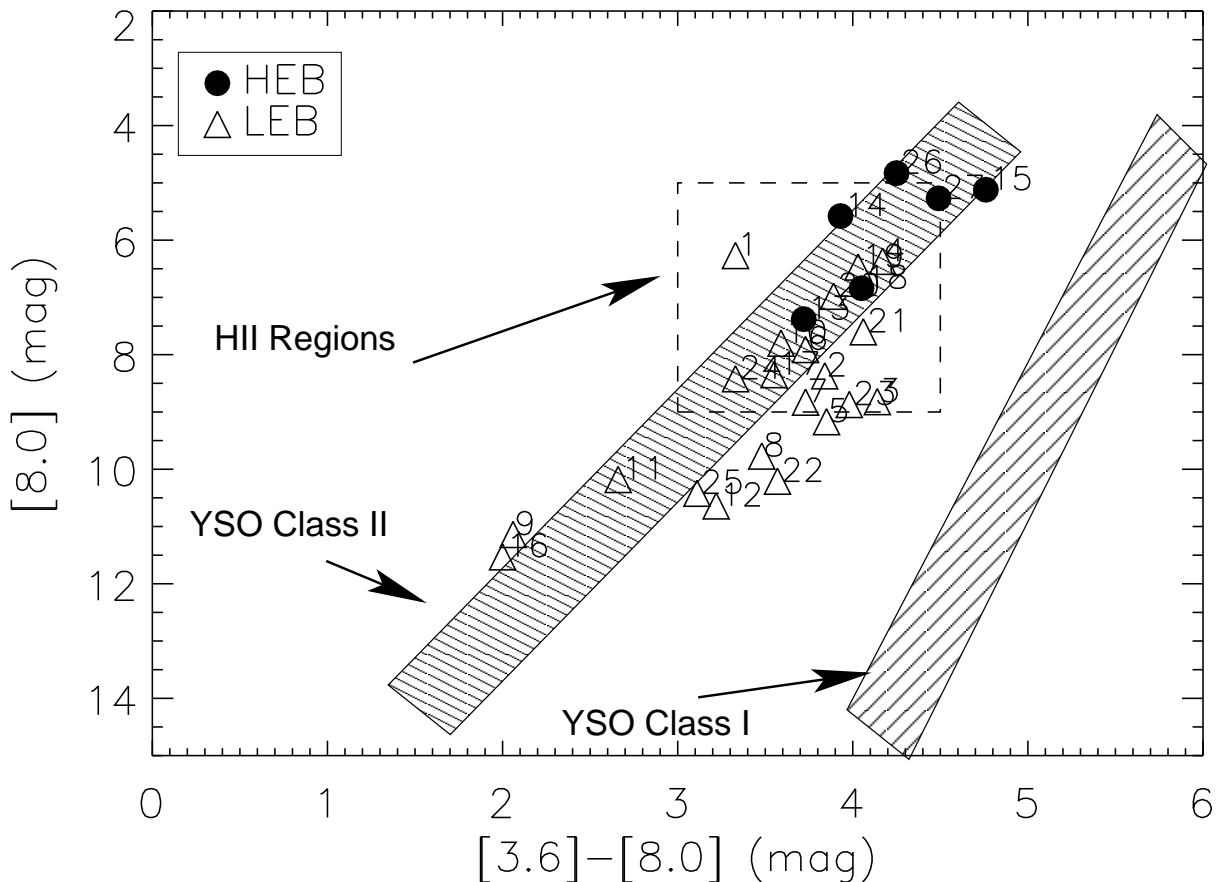


Fig. 3. The $8.0\ \mu\text{m}$ flux (in mags) as a function of the $[3.6]-[8.0]$ color. The expected location of typical Galactic H II regions as well as Class I and II low-mass YSOs is also included (see text). HEBs are marked with filled circles and LEBs with open triangles.

this showing this object not only of a higher level than SMC N81 (object #13), but also quite comparable to the brightest blobs in the LMC. Its dust content seems to be stronger in the bands below $8\ \mu\text{m}$. Among the LMC blobs, N11A (#18) is less luminous in the $8\ \mu\text{m}$ band, while its mid-IR colors indicate the presence of large quantities of dust, or increased PAH emission.

It also appears that the average $[3.6]-[8.0]$ color is bluer in LEBs suggesting a less dusty environment. LEBs tend to be more evolved since their exciting stars have disrupted the bulk of their associated molecular clouds. Moreover, they are found in more isolated regions of the LMC and SMC, and therefore the H I and CO column densities are on average lower.

Fig. 1 is particularly interesting in that it shows N11A to be situated in a giant mid-IR shell surrounding a cavity created by energetic photons of the OB association LH9, which occupies the central area of N11B (Hatano et al., 2006). The association of N11A with the shell is very likely not just a line of sight projection but there seems to be a physical connection between the two. N11A may therefore be a second generation object triggered by the ionization front due to the expansion of N11B according to the scenario first suggested by Elmegreen & Lada (1977). This suggestion is in agreement with Hatano et al. (2006), who find it quite likely that a new generation of stars be formed in peripheral regions of N11B from swept-up molecular clouds. Examples of triggered massive-star

formation at the border of Galactic H II regions have recently been discussed in the literature (e.g., Deharveng et al., 2005; Zavagno et al., 2007).

As we can see from Fig. 3, the colors of the sample compact H II regions are inconsistent with the locus of Class I YSO objects. There is though some overlap with the Class II objects (see also Gouliermis et al., 2007). However, we find it quite unlikely that each HEB or LEB in our sample be associated with a low-mass YSO. In their study, using Spitzer IRAC observations, Jones et al. (2005) detected a couple of Class I YSO candidates towards the LMC giant H II region N159, which spans over 5 arcmin on the sky, corresponding to 75 pc. Similarly, Gouliermis et al. (2007) found 22 candidate YSOs in their Spitzer study of the SMC H II region N90/NGC 602, which has a physical extent of about 70 pc. In comparison, the physical sizes of our sample blobs are around ~ 2 pc. Consequently, the probability that each H II blob harbors a low-mass YSO is very small, suggestion that the overlap of the Class II YSOs with the blobs in Fig. 3 is fortuitous.

In order to get a better insight on the infrared properties of our sample, we present in Fig. 4 the second diagnostic IRAC color-color diagram where the $[3.6]-[4.5]$ IRAC color is plotted as a function of the $[5.8]-[8.0]$ color. In this figure we mark again the expected loci of giant H II regions and YSOs based on the models of Allen et al. (2004) dealing with Galactic low-

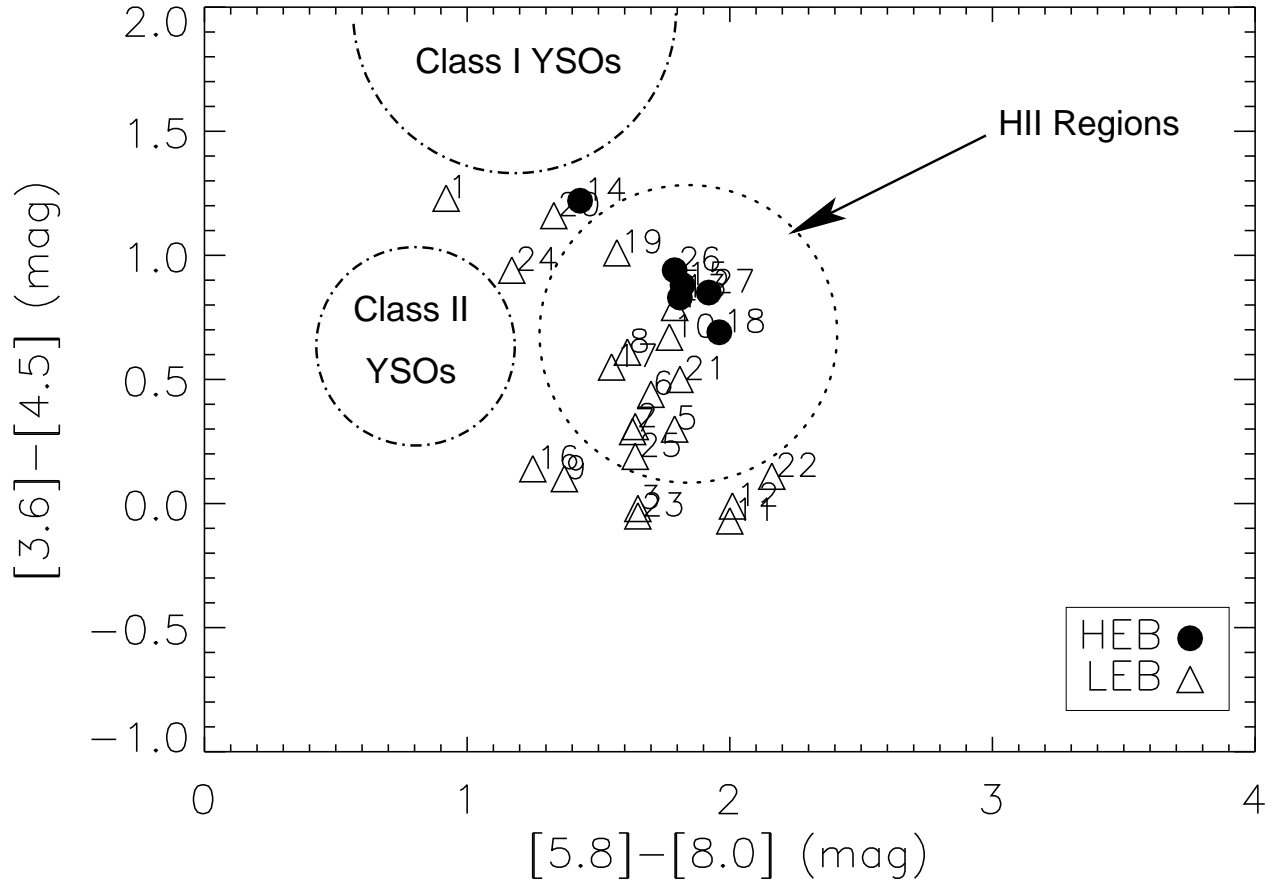


Fig. 4. The $[3.6]-[4.5]$ IRAC color as a function of the $[5.8]-[8.0]$ color. We also indicate the expected positions for YSOs as well as the locus of giant H II regions from the models of Allen et al. (2004). HEBs are marked with filled circles and LEBs with open triangles.

mass YSOs (see also Jones et al., 2005). We note that the YSOs are in principle readily separated from the compact H II regions. Extinction from dust though will have as an effect to move the data points of our sample towards the region occupied by Class I YSOs. This could be the reason for the colors of SMC-N10 (object #1). However, it seems unlikely that reddening be so substantial for the majority of the sample. Based on the work of Megeath et al. (2004) an $A_V = 30$ mag would move the H II points by 0.5 mag towards the locus of Class I YSOs. Our past optical and near-IR studies though suggest that the extinction towards the HEBs and LEBs does not reach these high values. The global mid-IR colors for some blobs of our sample (i.e. objects #3, #9, #23) are similar to those found in PDR regions. This deduction is based on the H II region results of (Zavagno et al., 2006) where they find that towards a pure filament devoid of any exciting star, the mid-IR colors are $[3.6]-[4.5] \sim 0.1$ mag and $[5.8]-[8.0] \sim 1.8$ mag. Elevated PAH emission can contribute to a red $[5.8]-[8.0]$ color while photospheric emission from stars results to a zero or negative $[3.6]-[4.5]$ color.

It is interesting to note that even though all compact H II regions in our sample have approximately the same size in the optical, their $H\alpha$ flux varies by nearly two orders of magnitude, with the HEBs being the more luminous (Meynadier & Heydari-Malayeri, 2007). Consequently their 8

μm emission, which has been shown to be correlated in general with to the $H\alpha$ emission (Wu et al., 2005; Calzetti et al., 2007), also spans over the same range, nearly 6 mags (see Fig. 3). Using the $H\alpha$ and the de-reddened $H\beta$ photometry of Meynadier & Heydari-Malayeri (2007), we searched for such a correlation for our sample. However, we found that these ratios exhibit a substantial scatter which is similar in both LEBs and HEBs. It is conceivable that this could be due to the small size of the compact H II regions and the fact that our Spitzer apertures do contain some mid-IR emission from the surrounding regions, as well as to uncertainties in the $H\beta$ extinction corrections.

5. Conclusions

Using Spitzer archival data we have explored the mid-IR properties for a sample of 27 high- and low-excitation compact H II regions in the Magellanic Clouds. This first study of the blobs in mid-IR is a necessary step towards understanding various aspects of these objects.

We find that in spite of their similar linear sizes (of just ~ 2 pc) the mid-IR colors of these objects are comparable to typical giant Magellanic Cloud H II regions. HEBs appear more luminous than LEBs at $8 \mu\text{m}$, which is consistent with their higher $H\alpha$ and $H\beta$ emission. HEBs are also on average redder since

they are younger and enshrouded in larger quantities of dust. No variations in the mid-IR colors were found to be correlated to metallicity or hardness of the radiation field of the sources. Although the loci of the blobs in the mid-IR color-magnitude plot overlap with low-mass YSOs of Class II, the probability that they contain such an object is estimated to be very low.

Acknowledgements. We would like to thank Dr. Lise Deharveng, Laboratoire d'Astrophysique de Marseille, for stimulating comments and discussions. VC would like to acknowledge partial support from the EU ToK grant 39965.

References

- Allen, L. E., et al. 2004, ApJS, 154, 363
 Bodenheimer, P., Tenorio-Tagle, G., & Yorke, H. W. 1979, ApJ, 233, 85
 Bolatto, A. D., et al. 2007, ApJ, 655, 212
 Calzetti, D., et al. 2007, ApJ, 666, 870
 Cesarsky, D., et al. 1996, A&A, 315, 329
 Churchwell, E. 1990, A&A Rev., 2, 79
 Cohen, M. 1993, AJ, 105, 1860
 Cohen, M. 2007, et al. MNRAS, 374, 979
 Deharveng, L., Zavagno, A., & Caplan, J. 2005, A&A, 433, 565
 Elmegreen, B. G., Lada, C. J., 1977, ApJ, 214, 725
 Fazio, G. G., et al. 2004, ApJS, 154, 10
 Förster Schreiber, N. M., Roussel, H., Sauvage, M., & Charmandaris, V. 2004, A&A, 419, 501
 Gouliermis, D. A., Quanz, S. P., & Henning, T. 2007, ApJ, 665, 306
 Hatano, H., Kadowaki, R., Nakajima, Y., et al. 2006, AJ132, 2653
 Heydari-Malayeri, M., Testor, G., 1982, A&A, 111, L11
 Heydari-Malayeri, M., Testor, G. 1983, A&A, 118, 116
 Heydari-Malayeri, M., Testor, G. 1985, A&A, 144, 98
 Heydari-Malayeri, M., Testor, G. 1986, A&A, 162, 180
 Heydari-Malayeri, M., Le Bertre, T., Magain, P. 1988a, A&A, 195, 230
 Heydari-Malayeri, M., Magain, P., Remy, M., 1988b, A&A, 201, L41
 Heydari-Malayeri, M., Van Drom, E., Leisy, P. 1990, A&A, 240, 481
 Heydari-Malayeri, M., Rosa, M. R., Zinnecker, H., Deharveng, L., & Charmandaris, V. 1999, A&A, 344, 848
 Heydari-Malayeri, M., Charmandaris, V., Deharveng, L., Martins, Rosa, M. R., Schaerer, D., & Zinnecker, H. 2001, A&A, 372, 527
 Heydari-Malayeri, M., Meynadier, F., Charmandaris, V., Deharveng, L., Le Bertre, T., Rosa, M. R., & Schaerer, D. 2003, A&A, 411, 427
 Heydari-Malayeri, M., Rosa, M. R., Charmandaris, V., Deharveng, L., Martins, F., Meynadier, F., Schaerer, D., & Zinnecker, H. 2007, ArXiv e-prints, 707, arXiv:0707.1209
 Israel F. P., Koornneef J., 1991, A&A, 248, 404
 Jones, T. J., Woodward, C. E., Boyer, M. L., Gehr, R. D., & Polomski, E. 2005, ApJ, 620, 731
 Lebouteiller, V., Bernard-Salas, J., Brandl, B., Whelan, D., Wu, Y., Charmandaris, V., & Devost, D. 2007, ArXiv e-prints, 710, arXiv:0710.4549
 Megeath, S. T., et al. 2004, ApJS, 154, 367
 Meixner, M., et al. 2006, AJ, 132, 2268
 Melena, N. W., Massey, P., Morrell, N. I., Zangari, A. M. 2008, AJ, 135, 878
 Meynadier, F., & Heydari-Malayeri, M. 2007, A&A, 461, 565
 Mirabel, I. F., et al. 1998, A&A, 333, 1
 Peeters, E., Hony, S., Van Kerckhoven, C., Tielens, A. G. G. M., Allamandola, L. J., Hudgins, D. M., & Bauschlicher, C. W. 2002, A&A, 390, 1089
 Tenorio-Tagle, G. 1979, A&A, 71, 59
 Testor, G., Pakull, M. 1985, A&A145, 170
 van Dishoeck, E. F. 2004, ARA&A, 42, 119
 Vermeij, R., Peeters, E., Tielens, A. G. G. M., & van der Hulst, J. M. 2002, A&A, 382, 1042
 Verstraete, L., et al. 1996, A&A, 315, 337
 Werner, M. W. et al. 2004, ApJS, 154, 1
 Whitney, B., Indebetouw, R., Bjorkman, J. E., & Wood, K. 2004, ApJ, 617, 1177
 Wolfire, M. G., Cassinelli, J. P. 1987, ApJ, 319, 850
 Wu, H., Cao, C., Hao, C.-N., Liu, F.-S., Wang, J.-L., Xia, X.-Y., Deng, Z.-G., & Young, C. K.-S. 2005, ApJ, 632, L79
 Zavagno, A., Deharveng, L., Comerón, F., Brand, J., Massi, F., Caplan, J., & Russeil, D. 2006, A&A, 446, 171
 Zavagno, A., Pomarès, M., Deharveng, L., Hosokawa, T., Russeil, D., Caplan, J. 2007, A&A, 472, 835
 Zinnecker, H., & Yorke, H. W. 2007, ARA&A, 45, 481

List of Objects

- 'SMC-N10' on page 8
 'SMC-N11' on page 8
 'SMC-N21' on page 8
 'SMC-N26' on page 8
 'SMC-N31' on page 8
 'SMC-N33' on page 8
 'SMC-N32' on page 8
 'SMC-N45' on page 8
 'SMC-N64' on page 8
 'SMC-N68' on page 8
 'SMC-N75' on page 8
 'SMC-N77' on page 8
 'SMC-N81' on page 8
 'SMC-N88A' on page 8
 'LMC-N83B' on page 8
 'LMC-N88' on page 8
 'LMC-N90' on page 8
 'LMC-N11A' on page 8
 'LMC-N191A' on page 8
 'LMC-N105A' on page 8
 'LMC-N193' on page 8
 'LMC-N33' on page 8
 'LMC-N197' on page 8
 'LMC-N68' on page 8
 'LMC-N156' on page 8
 'LMC-N160A2' on page 8
 'LMC-N159-5' on page 8

Table 1. Mid-IR photometry of the Compact H II Region Sample

ID	Region	RA (J2000)	Dec (J2000)	AORKEY	Source (mag)				Sky (MJy sr ⁻¹)			
					f _{3.6μm}	f _{4.5μm}	f _{5.8μm}	f _{8.0μm}	σ _{3.6μm}	σ _{4.5μm}	σ _{5.8μm}	σ _{8.0μm}
1	SMC-N10	0:44:56.4	-73:10:10.7	10740992	9.60	8.37	7.19	6.27	0.159	0.178	0.369	0.569
2	SMC-N11	0:45:00.2	-73:16:37.4	10740992	12.21	11.90	10.01	8.37	0.515	0.452	0.642	0.834
3	SMC-N21	0:47:53.1	-73:17:35.2	10740992	12.96	12.98	10.47	8.82	0.287	0.352	0.760	0.890
4	SMC-N26	0:48:08.6	-73:14:55.6	10740992	10.54	9.75	8.15	6.37	0.399	0.493	0.762	1.084
5	SMC-N31	0:48:41.9	-73:26:15.6	10740992	13.03	12.73	10.96	9.17	0.419	0.552	0.324	0.836
6	SMC-N33	0:49:28.9	-73:26:34.2	10743040	11.64	11.20	9.61	7.91	0.476	0.278	0.193	0.193
7	SMC-N32	0:49:40.9	-72:48:47.9	10741248	12.56	12.27	10.45	8.83	0.778	0.852	0.358	0.708
8	SMC-N45	0:51:40.7	-73:13:34.6	10743040	11.02	11.14	11.03	10.86	0.123	0.310	0.313	0.484
9	SMC-N64	0:58:16.8	-72:38:38.5	10741504	13.20	13.09	12.51	11.14	0.238	0.328	0.276	0.499
10	SMC-N68	0:58:42.9	-72:27:16.8	10741504	11.39	10.72	9.57	7.80	0.156	0.326	0.211	0.262
11	SMC-N75	1:02:31.6	-71:57:00.3	10742016	12.84	12.90	12.18	10.18	0.111	0.766	0.676	0.239
12	SMC-N77	1:02:49.2	-71:53:19.0	10742016	13.86	13.87	12.65	10.64	0.335	0.115	0.151	0.489
13	SMC-N81*	1:09:13.0	-73:11:38.3	10742528	11.10	10.27	9.19	7.38	0.091	0.652	1.049	1.466
14	SMC-N88A*	1:24:08.0	-73:09:03.9	4383488	9.51	8.29	7.01	5.58	0.040	0.028	0.086	0.123
15	LMC-N83B*	4:54:25.2	-69:11:03.2	14351616	9.88	9.00	6.94	5.12	0.152	0.274	0.271	0.331
16	LMC-N88	4:54:51.6	-69:23:24.4	14353152	13.53	13.39	12.77	11.53	0.308	0.109	0.142	0.151
17	LMC-N90	4:55:25.5	-69:16:06.4	14353152	11.89	11.35	9.90	8.35	0.509	0.091	0.501	0.170
18	LMC-N11A*	4:57:16.2	-66:23:20.8	14352128	10.89	10.20	8.79	6.84	1.409	1.010	1.331	2.478
19	LMC-N191A	5:04:37.5	-70:54:37.1	14354944	10.50	9.48	8.03	6.47	6.011	0.512	4.648	1.546
20	LMC-N105A	5:09:48.6	-68:52:44.0	14353664	10.87	9.71	8.31	6.98	0.473	0.508	0.907	0.955
21	LMC-N193	5:12:32.2	-70:24:19.3	14367488	11.66	11.16	9.40	7.60	0.097	0.123	0.166	0.247
22	LMC-N33	5:16:47.6	-67:19:38.4	14366464	13.79	13.68	12.38	10.21	0.088	0.148	0.357	0.454
23	LMC-N197	5:20:53.9	-71:43:16.1	14356736	12.85	12.90	10.52	8.87	0.780	0.073	0.572	0.266
24	LMC-N68	5:37:02.8	-68:14:11.0	14357504	11.76	10.81	9.59	8.42	0.120	0.053	0.765	0.574
25	LMC-N156	5:37:38.2	-69:34:25.4	14371584	13.53	13.34	12.06	10.42	0.418	0.342	0.311	0.957
26	LMC-N160A2*	5:39:46.1	-69:38:35.5	14371584	9.08	8.14	6.62	4.83	0.077	0.221	0.957	1.931
27	LMC-N159-5*	5:40:04.4	-69:44:37.4	14359040	9.76	8.91	7.19	5.27	0.651	0.520	1.120	1.464

Table note: The horizontal line separates the SMC and LMC sources. The high excitation blobs (HEBs) of our sample are indicated with an asterisk (*).